Advances in Water Resources 106 (2017) 24–38

Contents lists available at ScienceDirect

Advances in Water Resources

journal homepage: www.elsevier.com/locate/advwatres

Sugar-influenced water diffusion, interaction, and retention in clay interlayer nanopores probed by theoretical simulations and experimental spectroscopies

Ludmilla Aristilde[a,b,*], Stephen M. Galdi[a,1], Sabrina E. Kelch[b,1], Thalia G. Aoki[a]

[a] Department of Biological and Environmental Engineering, College of Agriculture and Life Sciences, Cornell University, Ithaca, NY 14853, USA
[b] Soil and Crop Sciences Section, School of Integrative Plant Science, College of Agriculture and Life Sciences, Cornell University, Ithaca, NY 14853, USA

ARTICLE INFO

Article history:
Received 1 June 2016
Revised 12 March 2017
Accepted 15 March 2017
Available online 18 March 2017

Keywords:
Soil nanopore
Water diffusion
Smectite clays
Mineral interlayers

ABSTRACT

Understanding the hydrodynamics in clay nanopores is important for gaining insights into the trapping of water, nutrients, and contaminants in natural and engineered soils. Previous investigations have focused on the interlayer organization and molecular diffusion coefficients (D) of cations and water molecules in cation-saturated interlayer nanopores of smectite clays. Little is known, however, about how these interlayer dynamic properties are influenced by the ubiquitous presence of small organic compounds such as sugars in the soil environment. Here we probed the effects of glucose molecules on montmorillonite interlayer properties. Molecular dynamics simulations revealed re-structuring of the interlayer organization of the adsorptive species. Water-water interactions were disrupted by glucose-water H-bonding interactions. "Dehydration" of the glucose-populated nanopore led to depletion in the Na solvation shell, which resulted in the accumulation of both Na ions (as inner-sphere complexes) and remaining hydrated water molecules at the mineral surface. This accumulation led to a decrease in both D_{Na} and D_{water}. In addition, the reduction in $D_{glucose}$ as a function of increasing glucose content can be explained by the aggregation of glucose molecules into organic clusters H-bonded to the mineral surface on both walls of the nanopore. Experimental nuclear magnetic resonance and X-ray diffraction data were consistent with the theoretical predictions. Compared to clay interlayers devoid of glucose, increased intensities and new peaks in the ^{23}Na nuclear magnetic resonance spectra confirmed increasing immobilization of Na as a function of increasing glucose content. And, the X-ray diffraction data indicated a reduced collapse of glucose-populated interlayers exposed to decreasing moisture conditions, which led to the maintenance of hydrated clay nanopores. The coupling of theoretical and experimental findings sheds light on the molecular to nanoscale mechanisms that control the enhanced trapping of water molecules and solutes within sugar-enriched clay nanopores.

1. Introduction

The unsaturated, or vadose, zone of soils plays an important role in mediating nutrient and water availabilities for plant and microbial biota, facilitating carbon sequestration, and capturing contaminants above drinking water aquifers. A crucial component influencing the fluid flow in the vadose zone is the trapping of fluids within nanopore regions of the soil environment (Tuller et al., 1999; Blunt et al., 2013; Sulman et al., 2014). Therefore, it is important to gain a fundamental understanding of the hydrodynamics that govern water and solute diffusion in soil nanopores. This understanding is required to inform the mechanistic framework underlying water and solute fluxes across different scales in the vadose zone (Bourg et al., 2007; Hallett et al., 2013; Tertre et al., 2015; Tinnacher et al., 2016). At the nanoscale, waters and associated solutes trapped in soil nanopores provide for long-term storage of soil moisture and nutrient content. Understanding the dynamics of this trapped water, particularly in drought-prone soils, is vital to predicting its role in maintaining long-term inaccessible soil moisture versus enhancing the residence of plant-available soil water (Sposito, 2013). In addition, solutes in nanopore-trapped environments within small particles can be subjected to meter-long transport through macropores (Smucker et al., 2007). Much attention has been devoted to studying the diffusion of waters and ions in the interlayer nanopore of minerals, particularly smectite clay minerals, due to the swelling capabilities of these minerals as well as their prevalence in environmental matrices (Bourg et al., 2007; Bourg and Sposito, 2011; Holmboe and Bourg, 2014).

* Corresponding author.
E-mail address: ludmilla@cornell.edu (L. Aristilde).
[1] These authors contributed equally to this manuscript.

http://dx.doi.org/10.1016/j.advwatres.2017.03.014
0309-1708/

However, little is known about the influence of the ubiquitous presence of small polar organic molecules such as sugars on hydrodynamic behaviors in smectite nanopores. Here we study the effects of glucose, the most common carbohydrate in soils (Paul and Clark, 1996), on the diffusion and retention of water and solutes within montmorillonite interlayer nanopores.

It has long been recognized that soil hydration and aggregation can be promoted by simple sugars and polysaccharides (Greenland, 1956; Greenland et al., 1962; Greenland, 1965; Olness and Clapp,1975; Pusino et al., 1989). For instance, clay and quartz minerals amended with polysaccharides exhibited higher rate of water retention than non-amended samples (Chenu, 1993). Enhanced water-holding capacity near plant roots relative to the bulk soil has been attributed to the mixture of secreted organic compounds with surrounded soil minerals (Carminati et al., 2011; Carminati et al., 2010). The secretion of mucilage, an agglomeration of sugar polymers, at the tips of roots is reported to increase hydraulic conductivity during dry conditions (Young, 1995; Read et al., 1999). This sugar secretion is also implicated in enhancing uptake of water and nutrients by plants (Paynel et al., 2013; Ahmed et al., 2014). Concentrations of low-molecular-weight organic compounds including glucose are only about 0.1 to 50 μM in bulk soil solutions (van Hees et al. 2005; Ryan et al., 2001; Fisher et al., 2007) but can be up to 10 mM in plant and microbial secretions in the rhizosphere and in organic matter-enriched soil patches (Veneklaas et al., 2003; Hodge, 2004; Lievens et al., 2015). Therefore, of special interest is the influence of these small organic compounds including sugars on water behavior in mineral soil nanopores, particularly in soil regions with high organic content.

Molecular-scale studies are lacking on the effects of glucose and other related small uncharged polar organics on water and solute hydrodynamics in clay nanopores. Prior molecular modeling studies have focused on elucidating the chemical interactions of surfactants, non-polar, and large organics on the mineral surface (e.g., Sutton and Sposito, 2006; Lee et al., 2013; Underwood et al., 2015; Zhang et al., 2016), and a few studies have also considered the connections of these interactions to diffusion properties (e.g., Zhao and Burns, 2013; Smaraweera et al., 2014). The application of molecular dynamics (MD) and Monte Carlo simulations has been widely employed for obtaining detailed insights on the factors controlling the molecular diffusion of water and metal ions in the interlayer nanopores of smectite clays such as montmorillonite (e.g., Chávez-Páez et al., 2001; Cygan et al., 2009; Botan et al., 2011; Bourg and Sposito, 2011; Holmboe and Bourg, 2014). The interlayer swelling of smectites is facilitated by the solvation of charge-compensating cations, which balance the permanent negative structural charges that arise from isomorphic substitutions in the clay structure (Sposito, 2008). The molecular organization of ion species at the mineral surface is described by the electrical double layer, which presents a structural framework for the formation of three statistical layers of adsorbate species at the mineral interface: inner-sphere complexes, outer-sphere complexes, and diffuse swarm species (Bourg and Sposito, 2010; Sposito, 2004; Tournassat et al., 2009). Using MD simulations, Bourg and Sposito (2011) conducted a detailed investigation of the electrical double layer for electrolyte solutions within montmorillonite nanopores. Their findings revealed that the specific localization of the three populations of adsorbed ions at the fluid-mineral interface, albeit very dynamic, determines molecular diffusion of these species (Bourg and Sposito, 2011; Holmboe and Bourg, 2014; Tinnacher et al., 2016).

Notably, adsorbed cation species (Na^+, Ca^{2+}) in close associations with the mineral surface are reported to exhibit slower molecular diffusion than recorded for those species diffusing in bulk liquid solutions (Marry et al., 2008; Bourg and Sposito, 2011; Zhang et al., 2014; Tertre et al., 2015). For instance, the molecular diffusion coefficient (D) for the first layer of Na ions and water molecules at the fluid-mineral interface was, respectively, 85% and 44–60% lower than the D value obtained in bulk liquid (Bourg and Sposito, 2011). Furthermore, it was stressed previously that reduction in water diffusion may be due to reduced mobility of waters accompanying the metal cations localized close to the fluid-mineral interface in the nanopores (Sposito, 1982; Bourg and Sposito, 2011; Zhang et al., 2014). Based on a kinetic model of MD results, Marry et al., (2008) proposed more rapid H-bond formation between waters and the surface than H-bond dissociation. This is consistent with a previous proposal that H-bonds between the first statistical layer of water molecules and O atoms at the mineral surface contribute to the decreased mobility of water (Sposito, 1982). Therefore, both the water structure and the water relationship with metal cations at the fluid-mineral interface dictate the water diffusion in smectite nanopores.

In this study, we seek to shed light on the response of the water and solute diffusion dynamics in smectite nanopores to the presence of glucose. We hypothesized that the presence of glucose molecules may alter the hydrodynamic behavior in the interlayer nanopores of Na-montmorillonite in four main ways: (1) perturbation in the localization of adsorbed Na^+ species at the fluid-mineral interface alters Na diffusion, (2) changes in hydration at the mineral basal surface influence the water diffusion profile, (3) glucose-water interactions disrupt water-water interactions, and (4) glucose interaction on the mineral surface impedes glucose diffusion.

Relevant to the first three hypotheses, previous MD simulations of a model natural organic matter in a Ca-montmorillonite nanopore pointed out that the large organic molecules promoted the formation of inner sphere complexes of Ca^{2+} on the mineral surface (Sutton and Sposito, 2006). This phenomenon was attributed to possible dehydration of the solvation shell of the cation due to disruption of the water structure in the presence of the organic molecules in the interlayer space (Sutton and Sposito, 2006). By contrast to the organic polymer used in this previous simulation, the relatively smaller size of glucose may lead to different disruptions in the organization of both cations and water molecules in clay interlayer nanopores. The application of solid-state nuclear magnetic resonance (NMR) has been instrumental in capturing the dynamics of Na^+ species at mineral surfaces (Grandjean, 2001) and intermolecular interactions proposed within simulated montmorillonite nanopores populated by small polar organic compounds (Hellrup et al., 2016; Aristilde et al., 2016; Aristilde et al., 2010). This spectroscopic approach may therefore be useful in capturing dynamic changes in interlayer solutes in glucose-populated interlayers.

With respect to the fourth hypothesis, previous density functional theory (DFT) calculations reported H-bond formation of glucose with the siloxane surface of kaolinite (Lee et al., 2013). Previous MD simulations of alkyl hydrocarbons with or without a polar group (Underwood et al., 2015; Zhang et al., 2016) reported that these organics coalesced together and avoid interactions with the mineral surface in a Na-montmorillonite nanopore. Diffusion of non-polar benzene was found to be slowed down significantly within a montmorillonite interlayer nanopore populated by a cationic surfactant (Zhao and Burns, 2013). Intermolecular interactions between the different organic entities were implicated in disrupting the diffusivity of benzene within the montmorillonite interlayer space (Zhao and Burns, 2013). Interestingly, with respect to glucose, it was found that glucose adsorption energy on the hydroxyl-containing surface of kaolinite was greater than on the siloxane surface due to increased H-bond formation (Lee et al., 2013). Therefore, the flocculation of polar glucose molecules via multiple intermolecular H-bonding interactions is likely given the

strong attraction of glucose to hydroxyl surfaces. The potential influence of these intermolecular interactions on the diffusion of both water and glucose in clay nanopores has not yet been evaluated.

X-ray diffraction (XRD) has been employed to investigate water behaviors in smectite clay interlayers experimentally (Ferrage et al., 2005; Ferrage, 2016). The hydration states of cation-saturated montmorillonite interlayers are manifested structurally by expansion of the layer-to-layer distance or d_{001} (Ferrage, 2016). Stepwise increase in d_{001} of montmorillonite as a function of increasing relative humidity (RH) represents the increasing inclusion of layers of water molecules (up to 4) in the clay nanopore (Ferrage et al., 2005; Holmboe and Bourg, 2014; Ferrage, 2016). The range of d_{001} achieved at each step that corresponds to the incorporation of each additional water layer has been well defined for metal cation-saturated smectite clays (Ferrage, 2016): 1.18–1.29 nm d_{001} for mono-hydrated, 1.45–1.58 nm d_{001} for bi-hydrated, and 1.80–1.95 nm d_{001} for tri-hydrated layers. A four-hydrate layer with d_{001} 2.15–2.20 nm was reported for when the water saturation of the clay was proceeded from liquid water (Holmboe and Bourg, 2014). The monitoring of d_{001} using XRD measurements has provided insights on the effects of the type of interlayer cations (i.e. Na^+, K^+, Ca^{2+}, Mg^{2+}) on the evolution of hydration states in smectite nanopores (Ferrage et al., 2005; Ferrage, 2016). In conjunction with the d_{001} values, the full width at half maximum intensity (FWHM) of the 001 reflection allows monitoring of the interstratification of the different hydrated layer types (Ferrage et al., 2005). An increase in the heterogeneity of the interstratified montmorillonite layers without or with intercalated organic molecules results in an increase in FWHM (Ferrage et al., 2005; Aristilde et al., 2013). In the case of cation-saturated montmorillonite interlayers (Ferrage et al., 2005), FWHM was the largest when the recorded d_{001} was in-between the d_{001} values defined for a specific hydration state (as described above) due to the simultaneous presence of the different layer types at different proportions. In light of previous observations that sugar-enriched bulk soils or clay nanoparticles led to enhanced water retention, it is warranted to understand the interlayer hydrodynamics with respect to shifting hydration states and interstratified interlayer types in glucose-populated nanopores.

We present here an evaluation of our four hypotheses stated above by making use of molecular modeling simulations supplemented with both NMR and XRD measurements to probe the response of both diffusion and retention of water and solutes in the clay interlayer nanopores populated by glucose. We combined Monte Carlo and MD simulations to model Na-montmorillonite at 2-nm d_{001} populated with two scenarios of glucose content wherein 5% or 20% of the pore volume was occupied by glucose molecules. For comparative analysis, we also conducted simulations in the absence of glucose and the simulation results with glucose-free nanopores were consistent with prior molecular simulations. Using the MD-optimized systems, we determined the molecular diffusion, interlayer organization, and intermolecular interactions of solutes and water molecules in the montmorillonite interlayers. Solid-state ^{23}Na NMR spectra revealed dynamic changes in Na populations due to glucose enrichments. The XRD data were obtained as a function of *in* situ equilibration of the clay interlayers to different moisture conditions. The present findings shed light on the implications of fluids trapped in sugar-containing nanopores for mass fluxes of water molecules and solute species in the nanopore regions of the vadose zone.

2. Methodology

2.1. Modeling platform

For the molecular simulations, we used the all-atom forcefield COMPASS (Condensed-phase Optimized Molecular Potentials for Atomistic Simulation Studies; San Diego, CA) as implemented in the Materials Studio software package (Accelrys, 2013). The partial charges of the atoms in water molecules and the montmorillonite structure were according to, respectively, the extended simple point charge water model (Berendsen et al., 1987) and the CLAYFF model (Cygan et al., 2004). All other atom descriptions including bonding and nonbonding terms were assigned by the COMPASS forcefield (Sun, 1998). The nonbonding terms are represented by Lennard–Jones 6–12 and coulomb potentials (Sun, 1998). Long-range coulombic interactions were evaluated using the Ewald summation method, as done previously for simulated montmorillonite nanopores (Bourg and Sposito, 2011). The COMPASS forcefield has been used previously for appropriate simulations of montmorillonite (Sutton and Sposito, 2006; Aristilde et al., 2010; Aristilde et al., 2013), metal cation hydration (Sutton and Sposito, 2006; Aristilde and Sposito, 2008), and various organic molecules (Sutton et al., 2005; Aristilde and Sposito, 2008; Aristilde and Sposito, 2010; Aristilde et al., 2013; Pochodylo et al., 2016).

2.2. Validation of glucose simulation

We subjected hydrated glucose to a series of simulations consisting of geometry optimization, energy minimization (EM), and annealing molecular dynamics, as previously described (Sutton et al., 2005; Aristilde and Sposito, 2008). Structural data were retrieved from a molecular dynamics production run which ran for 500 ps (time step = 1 fs). This final molecular dynamics run was carried out in a canonical NVT ensemble (fixed number of atoms, simulation cell volume, and constant temperature) using a canonical Berendsen thermostat algorithm to control temperature at 298 K. The potential energy profile indicated that equilibrium was reached after 50 ps. Bond lengths and bond angles were retrieved during the molecular dynamics production run after energy equilibration and subsequently compared with published X-ray structural data for glucose (Chu and Jeffrey, 1968). Bond lengths and bond angles (12 bond lengths and 14 bond angles) of the optimized configurations of glucose were all in agreement with published structural data (Chu and Jeffrey, 1968) [Supplementary Information (SI), Appendix A].

2.3. Molecular modeling simulations

The model basal clay surfaces were composed of a Wyoming-type model montmorillonite with (average) stoichiometry $Na_{0.5}(Si_8)(Al_{3.5}Mg_{0.5})O_{20}(OH)_4$ for the unit cell. The periodic $42.24 \times 36.56 \times 20.00$ Å^3 supercell contained a total structural charge of −16 arising from isomorphic substitutions (Al→Mg) scattered randomly in the octahedral sheet; there were no adjacent substitution sites according to the Loewenstein's rule (Loewenstein, 1954). The 2-nm d_{001} was chosen for simulating the hydrated montmorillonite interlayer for two reasons: (i) as stated in the introduction, the maximum reported for tri-hydrated smectites was 1.95 nm d_{001}; (ii) our XRD measurements revealed a maximum d_{001} of ~1.6 nm for glucose-filled montmorillonite interlayers equilibrated under 90% RH (see *Section 2.5*) and we thus expected a higher d_{001} would result at 100% RH. Charge-balancing counterions (i.e. 16 Na^+) were added in the interlayer space when constructing the three types of interlayer nanopores at 0.1 M NaCl ionic strength without and with increasing amounts of glucose compounds (4 or 16) (SI, Appendix B). Due to the small volume of the pore space, only one Na^+ and one Cl^- were inserted in the nanopore to reflect the 0.1 M NaCl.

Predicted statistical water monolayers at specific pore sizes have been previously used to determine water content in hydrated Na-montmorillonite layers (Fu et al., 1990; Sato et al., 1992; Holmboe and Bourg, 2014; Tamura et al., 2015). At 2-nm d_{001}, about 16 H_2O per unit cell [i.e., per $O_{20}(OH)_4$] is typically inserted

to account for 3 to 4 statistical monolayers of water molecules in the interlayer (Holmboe and Bourg, 2014). With the introduction of the sugars in the interlayer environment, this straightforward approach of determining the water content is problematic because the sugars can interface with the mineral surface such that the basal atoms in the unit cell are not all available to be "hydrated" by the interlayer water. As an alternative approach, we obtained the water content on a pore volume basis (i.e., the volume not occupied by non-water adsorptives) both in the presence and absence of sugars. It was proposed previously that water content greater than 10 water molecules per unit cell yields an interlayer water density of 1 kg dm^3 (Holmboe and Bourg, 2014). Therefore, at 16 H_2O per unit cell at 2-nm d_{001}, this water density was used to calculate the amount of water molecules in the pore volume. First, the allowable pore volume to be occupied by the adsorptives (Na, Cl, glucose, and water) was determined by obtaining the solvent-accessible surface in the interlayer space using an implemented algorithm in Materials Studio. Volume of the void to be occupied by the water molecules, which is the difference between the interlayer accessible volume and the Connolly volume of non-water adsorptives, was calculated to determine the number of water molecules to be added given the aforementioned interlayer water density. Table S1 (SI, Appendix B) lists the quantity of adsorptives, including water molecules, simulated in each interlayer nanopore.

Previous simulations have been conducted using a NVE ensemble (fixed number of atoms, fixed volume, and constant energy) with no volume optimization (Bourg and Sposito, 2010) or a NPT ensemble (fixed number of atoms and pressure, and constant temperature) wherein a volume optimization was allowed (Holmboe and Bourg, 2014; Bourg and Sposito, 2011). Acknowledging that water and solute diffusions are dependent on the mineral pore size (Kerisit and Liu, 2009; Holmboe and Bourg, 2014), all the molecular simulations here were carried out in a canonical NVT ensemble (fixed number of atoms, fixed simulation cell volume, and constant temperature) to evaluate the effects of glucose on water and ion diffusion within the same pore volume. We were encouraged that our simulation procedure was adequate due to good qualitative agreement of our MD predictions with previous simulations conducted in a NPT ensemble (See Section 3. Results).

A fully-rigid clay structure was used in all the simulations here. Previous MD simulations of Na-montmorillonite interlayers reported that the diffusion and density profiles of molecular species in highly-hydrated nanopores, as illustrated here, were minimally affected by the flexibility or rigidity of the clay structure (Holmboe and Bourg, 2014). It can be computationally expensive to obtain both geometry-optimization and energy-optimization during the MD relaxation step of the adsorptives in the nanopore. To lessen this expense significantly, we first employed a Monte Carlo search, following the general procedure delineated previously (Aristilde et al., 2010; Aristilde et al., 2013; Pochodylo et al., 2016) to obtain preliminary geometrically-optimized and energy-minimized arrangement of the adsorptives in the nanopore. This preliminary step employed the Adsorption Locator module in the Materials Studio software wherein all the adsorptives (see SI, Appendix B) were subjected simultaneously to both translation and rotation steps with respect to the montmorillonite basal surface over a temperature cycle, using a Berendsen thermostat, from 300 K to 600 K, repeated twice. Different conformations of the adsorptives in the interlayer were tested during this annealing adsorption procedure while simultaneously optimizing interaction energies. The lowest-energy nanopore obtained from this preliminary Monte Carlo step was subsequently subjected to a 1-ns MD pre-equilibration step using the Forcite module in the Materials Studio software (Fig. 1). Following this pre-equilibration, a MD production run was obtained by running an additional MD for 10 ns, at 5 fs time step and 298 K, using the Forcite module. This series of Monte Carlo and MD algorithms was conducted to attain thermodynamically-equilibrated adsorbate structures.

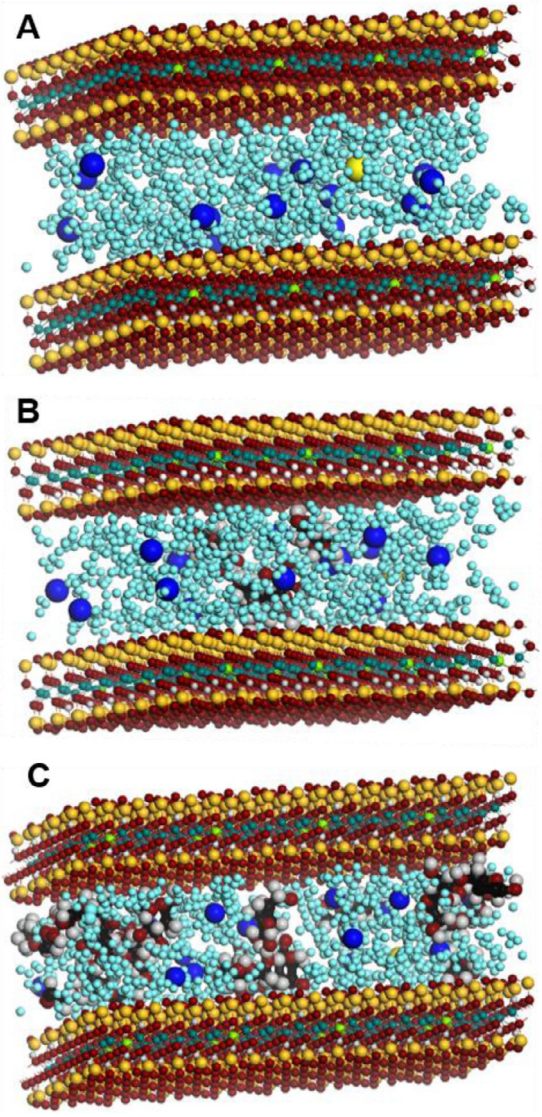

Fig. 1. Snapshot of the pre-equilibrated systems (1 ns) with 0.1 M NaCl solution confined in an interlayer at 2 nm d_{001} in the absence (A) and in the presence of 4 glucose molecules (B) and 16 glucose molecules (C). Color legend: O (red), H (white), Si (dark yellow in the clay structure), dark green (Al), light green (Mg), Na (dark blue), Cl (yellow in the interlayer), water molecules (light blue). (For interpretation of the references to colour in this figure legend, the reader is referred to the web version of this article.)

2.4. Analysis of molecular dynamics results

The MD-equilibrated configurations obtained during the 10-ns MD production run were used to compute the molecular-scale diffusion coefficient, the density profile of each solute, the intermolecular structural arrangements, and intermolecular and interfacial H-bond networks.

The fluxes of water and solutes through soil nanopores are governed by D, which has been determined from previous MD simulations of hydrated clay interlayers (Bourg and Sposito, 2013; Holmboe and Bourg, 2014) by using the Einstein relationship (Liu et al., 2004):

$$D_m = \frac{1}{2n} \lim_{\tau \to \infty} \frac{d\langle l^2 \rangle}{d\tau} \quad (1)$$

wherein the mean-square displacement, $\langle l^2 \rangle$, is calculated for a diffusing molecule m over the total number of molecules m, N_m, for the linear portion of the plot of $\langle l^2 \rangle$ versus 500-ps time intervals of τ for 7.5 to 10 ns; n represents the dimensionality of the systems. The following equation was used to determine $\langle l^2 \rangle$:

$$\langle l^2 \rangle = \sum_{i=1}^{N_m} \frac{|r(t) - r(t+\tau)|^2}{N_m} \quad (2)$$

for $r(t)$, the position of m at time t, during all time intervals τ. In MD simulations of large montmorillonite interlayer nanopores, non-constant localization (i.e., the anisotropy) highlighted the challenge in applying Eq. (1) for obtaining discriminate values for the two components of the diagonal tensor D, which consists of D parallel and normal to the mineral surface (respectively, $D_{\parallel}$ and $D_{\perp}$) (Botan et al., 2011; Holmboe and Bourg, 2014). However, in small interlayer nanopores sizes ($\leq$2 nm), D of water and solutes in the interlayer is controlled primarily by the basal clay surfaces on the side of the nanopores such that $D_{\perp}$ is negligible compared to $D_{\parallel}$. Therefore, for our system, it was adequate to calculate one overall D_m (i.e, D_{water}, D_{Na}, $D_{glucose}$), which encompasses the magnitude of the D vector of each m set, within the interlayer.

For each simulated system, we also obtained detailed information on the dynamic structural arrangements of molecules. We first captured the dynamic spatial distribution of Na, O_{water}, and $O_{glucose}$ in the interlayer space over the 10-ns MD production run at 1-ns time intervals. Then, density profiles for each species were determined as a function of z-coordinates, in the direction perpendicular to the mineral surface. Here we opted to monitor the position of only O_{water} (and not H_{water}) to obtain comparisons with the positioning of Na ions, which are solvated by O_{water} in the interlayer. The final plotted z-coordinate data were compiled at 0.07 nm intervals in the interlayer as time-averaged values at 1-ns time intervals over the total 10 ns MD run; fluctuations over the MD time course were represented by standard deviation values.

Secondly, to monitor the local structural environment, we calculated the isotropic radial distribution functions (RDFs) for the following atom pairs: H_{water}—O_{water}, H_{water}—O_{clay}, Na—O_{water}, Na—O_{clay}, H_{water}—$O_{glucose}$, $H_{glucose}$—O_{water}, $H_{glucose}$—O_{clay}. The RDFs were determined mathematically by pair correlation functions, $[g(r)]$, for atom b surrounding central atom a as follows (Allen and Tildesley, 1987):

$$g_{ab}(r) = \frac{1}{4\pi r^2 (N_b/V)} \frac{dN_{ab}}{dr} \quad (3)$$

As described, $g(r)$ provides a probability measure of finding atom b around atom a in a spherical shell of infinitesimal thickness dr. Thus, dN_{ab} is the average number of b surrounding a between the radial distance of r and $r+dr$. A dr interval of 0.02 Å was used in determining $g(r)$ from our MD simulation results. The number density of atoms b in the simulated cell content is represented by N_b/V, with V encompassing the supercell volume. The coordination number (CN) of atom b around atom a was computed by integrating the RDFs up to 6 Å. Integration to the first minimum, which occurred between 1.3 Å and 3.3 Å depending on the coordination relationship, provided well-defined first-shell coordination. Longer-range coordination or structural arrangement was calculated at greater distances from the central atom.

Thirdly, we determined the changes in the network of H-bonding as a function of added glucose in the interlayer. Of relevance to the water structure in the nanopore, three types of H-bonds were monitored: water-water H-bonds, water-clay H-bonds, and water-glucose H-bonds. Of relevance to glucose organization in the interlayer, we also monitored the glucose-glucose H-bonds and glucose-clay H-bonds. These intermolecular H-bonds were determined using the default criterion in the modeling software (Accelrys, 2013): a maximum H-acceptor distance of 2.0 Å and a minimum donor-H-acceptor angle of 120° The distance criterion falls within the range used in previous studies (< 3.5 Å) (Marry et al., 2008; Laage et al., 2006). The angle criterion chosen here has been used previously to track both intramolecular H-bonds within a flexible organic polymer or peptides as well as their intermolecular H-bonds with solvated water molecules (Sutton et al., 2005; Pochodylo et al., 2016). However, this angle criterion is larger than the one used in previous simulations of bulk water liquids (Laage et al., 2006). The more stringent angle criterion was not used here both to account for the dynamics of the glucose molecules and the fluctuations in the positions of the water atoms over the course of the MD run of our simulated systems.

2.5. Solid-state NMR and XRD measurements

To obtain qualitative experimental insights into the interlayer molecular interactions and hydration behavior predicted by the MD simulations, we performed both NMR and XRD analyses of montmorillonite following reactions with glucose-containing solutions at different glucose concentrations. The Wyoming Na-montmorillonite sample (SWy-2) was obtained from the clay repository of the Clay Mineral Society (West Lafayette, Indiana, USA) and used as received. The structural formula of the purchased MONT was reported as $(Ca_{0.12}Na_{0.32}K_{0.05})[Al_{3.01}Fe(III)_{0.41}Mn_{0.01}Mg_{0.54}Ti_{0.02}][Si_{7.98}Al_{0.02}]O_{20}(OH)_4$, with an octahedral charge of −0.53 and a tetrahedral charge of −0.02. The adsorption experiments (two to three replicates) were carried out by reacting aliquots (50 mL) of different glucose concentrations (0, 0.5, 2, 20 mM) with Na-montmorillonite (2 g/L) for 96 h in a 50 mL polypropylene centrifuge tubes. The glucose solutions were prepared in 0.1 M NaCl and 0.02 M $NaHCO_3$ buffer adjusted to pH 6.5. Following reaction time of 96 h, the slurries were centrifuged (2000 g, 20 min). These experiments were designed to obtain different glucose content scenarios in the composites in order to obtain preliminary corroboration of the theoretical predictions deduced from our MD simulations. Determining the exact glucose content in the glucose-clay composites was beyond the scope of the present study.

For the NMR measurements, the supernatant was completely removed following the centrifugation step and the samples were subsequently freeze-dried for 24 h. Solid-state ^{23}Na NMR spectra were recorded using an INOVA 400 instrument with a broadband DDProdigy Cryoprobe under automation using standard Bruker water suppression parameters on samples packed into a 4 mm diameter cylindrical zirconia rotor. The ^{23}Na magic angle spinning NMR spectra were obtained with a $\pi/8$ pulse duration of 0.75 µs, 1 s recycle delay and a spinning frequency of 12 kHz. For analysis, VNMRJ 1.1B and MNOVA software modules were used in analysis.

For the XRD measurements, the clay slurry prepared with 5 mL of the supernatant following the centrifugation step was pipetted on top of a flat sample holder. The sample holder was subsequently placed in an encased humidity-controlled chamber. Prior to recording XRD patterns, the sample was equilibrated in the chamber at constant temperature (25 °C) and, in decreasing order, at three different RH conditions generated *in situ*: 90%, 50%, and 20%. The RH and temperature conditions were maintained throughout the duration of the XRD acquisition. The XRD patterns were recorded with a Bruker D8 Advance powder X-ray diffractometer operated at 40 kV and 40 mA. The diffractometer was equipped with an Anton Parr Eurotherm TCU110 temperature control unit and an Anton Paar CHC+ temperature and humidity chamber with an attached ProUmid MHG-32 Modular Humidity Generator. The scanning parameters were 0.02° 2θ step size and 8 s as counting time per step over the $1.5 - 8.5°$ 2θ Cu Kα angular range (λ = 1.5406 Å). The XRD data were recorded at low-angle 2θ values because the focus

Table 1
Molecular diffusion coefficients (10^{-9} m^2 s^{-1}) of water molecules and solutes[a].

	Experiments with bulk water[c]	Previous MD simulations of bulk water[d]	Previous MD simulations of clay interlayer nanopores[e]			MD-predicted values determined in the present study[f]		
	298 K	298 K	d_{001} = 1.88 nm, 298 K	d_{001} = 1.88 nm, 323 K	d_{001} = 4.07 nm, 298 K	d_{001} = 2.0 nm, 298 K		
$Gluc_{conc}$[b]	0	0	0	0	0	0	0.5 mM	2 mM
D_{water}	2.54 (2.299)	2.68 ± 0.03	1.31 ± 0.03	2.19 ± 0.07	1.91 ± 0.02	1.92 ± 0.08	1.63 ± 0.01	0.92 ± 0.08
D_{Na}	1.335	1.08 ± 0.08	0.53 ± 0.05	0.79 ± 0.11	0.77 ± 0.15	0.74 ± 0.13	0.45 ± 0.10	0.17 ± 0.05
$D_{glucose}$	–	–	–	–	–	–	0.17 ± 0.07	0.042 ± 0.012

[a] MD data are reported as average ± standard deviation.
[b] Concentration of glucose ($Gluc_{conc}$) in the mineral nanopore.
[c] Experimental bulk diffusion coefficient values are from Talekar (1977) or Holz et al. (2000). The D_{water} from the most recent reference is shown between parentheses.
[d] Reported by Holmboe and Bourg (2014).
[e] Determined by Holmboe and Bourg (2014) using MD simulations of Na-montmorillonite at d_{001} = 1.88 nm and 4.07 nm
[f] Calculated in the present study using MD simulations of Na-montmorillonite at d_{001} = 2.0 nm.

here was on monitoring the 001 peak, from which the d_{001} (i.e., layer-to-layer distance) can be calculated. The FWHM was also determined for each 001 peak in order to monitor the changes in the heterogeneity of the interstratified montmorillonite layers formed under the different RH conditions (Ferrage et al., 2005; Aristilde et al., 2013).

3. Results

3.1. Molecular diffusion coefficients

Holmboe and Bourg (2014) reported that, relative to their MD-simulated bulk D values that were in close agreement with experimental data at 298 K (Talekar, 1977; Holz et al., 2000), there was a decrease in both D_{water} and D_{Na} in simulated montmorillonite nanopores of 1.88 nm d_{001} at the same temperature (see data presented in Table 1). Specifically, with their simulated systems at 1.88 nm d_{001}, D_{water} was decreased by 43% and D_{Na} by 60% relative to their reported corresponding D values in bulk liquid (Holmboe and Bourg, 2014) (Table 1). At 298 K, we also found that our D values for D_{water} and D_{Na} in the no-glucose montmorillonite interlayer of 2 nm d_{001} were less than the experimentally-determined bulk D values. (see Table 1). Relative to the experimentally-determined bulk D values, our nanopore D_{water} was decreased by 16% and the D_{Na} was decreased by 45% (Table 1).

At the same temperature (298 K), our MD-predicted D values with montmorillonite interlayer simulated at 2 nm d_{001} were greater than the MD-predicted values reported by Holmboe and Bourg (2014) at 1.88 nm d_{001} (Table 1). This discrepancy could be due to three main reasons. First, the annealing temperature cycle (from 300 K to 600 K and back to 300 K), which preceded the MD simulations conducted at 298 K, may have conditioned the solutes in the interlayer to higher-temperature dynamic behavior (See Methods section for details). Our D_{water} and D_{Na} values from our MD-simulated interlayers at 298 K were in close agreement with the MD-predicted values obtained by Holmboe and Bourg (2014) at 353 K from a Na-montmorillonite nanopore at d_{001} = 1.88 nm (Table 1). Second, the d_{001} (2 nm) of our simulated montmorillonite interlayers was 0.12 nm larger than the d_{001} montmorillonite interlayer simulated by Holmboe and Bourg (2014). As illustrated in Table 1, using simulations of montmorillonite interlayers at higher d_{001} (4.07 nm versus 1.88 nm), Holmboe and Bourg (2014) obtained higher D values for both Na and water molecules. Interestingly, our D values determined at 2 nm d_{001} closely matched the ones determined by Holmboe and Bourg (2014) at 4.07 nm d_{001}. Third, code-specific differences such as different ion pair potentials, different cutoffs and different treatment of the long-range interactions may have affected the calculated D values (Bourg and Sposito, 2010; Holmboe and Bourg, 2014). The MD-predicted D values in the montmorillonite interlayers simulated by Holmboe and Bourg (2014) may be underestimates due to the specific pair potentials used in their model. We note that as listed in Table 1 for bulk D values at 298 K, the bulk D_{water} determined from the simulations by Holmboe and Bourg (2014) was within 4% of an experimentally-determined value but the MD-determined bulk D_{Na} was up to 25% less than the experimental value. In any case, we found that the ratio for our MD-predicted D_{water} over D_{Na}, 2.59 ± 0.30, was congruent with the corresponding ratio determined at the different nanopores simulated by Holmboe and Bourg (2014): 2.47 ± 0.16 at 1.88 nm d_{001} and 298 K, 2.77 ± 0.26 at 1.88 nm d_{001} and 323 K, and 2.48 ± 0.38 at 4.07 nm d_{001} and 298 K.

Our MD data indicated that the influence of glucose presence on D_{water} and D_{Na} was dependent on the glucose concentration in the montmorillonite nanopore (Table 1). At the lowest glucose concentration (0.5 mM) investigated with our simulations, D_{water} was reduced by 15.1 ± 2.90% and D_{Na} by 39.2 ± 2.41% when compared to the corresponding D values determined with the simulated nanopore without any glucose (Table 1). When the glucose concentration was four times higher (i.e., 2.0 mM) in the nanopore, the D_{water} and D_{Na} values were, respectively, 52.08 ± 2.08% and 77.03 ± 2.31% less than the corresponding D values determined in the absence of glucose (Table 1).

We also obtained $D_{glucose}$ in both glucose-containing nanopores (Table 1). The four-fold increase in glucose concentration in the montmorillonite nanopore resulted in a 75.29 ± 2.21% decrease in $D_{glucose}$ (Table 1). Thus, increasing concentration of glucose in the montmorillonite nanopore promoted the reduced mobility of both water molecules and solutes. To gain further insights on this phenomenon, we monitored changes in the structural dynamics in the interlayer at the two different populations of glucose, and make comparisons to the dynamics in the absence of glucose.

3.2. Adsorptive density profiles

We investigated the localization of the adsorptives in the interlayer nanopore via density profiles along the z direction (Fig. 2). Fluctuations in the localization of the adsorptives, as captured by the dynamic standard deviation of the density profiles, allowed monitoring of the influence of glucose in constraining the molecular movement of the adsorptives in the interlayer (Fig. 2). The least variable density profiles for the water dynamics occurred in the simulated nanopores without any glucose or in the high-glucose nanopore with 16 glucose molecules (Fig. 2A and C); the most variable density profile was obtained in the interlayer with the lowest glucose population or 4 glucose molecules (Fig. 2B). In the clay nanopore devoid of glucose, the interlayer water density profile was characterized by two high-abundance peaks vici-

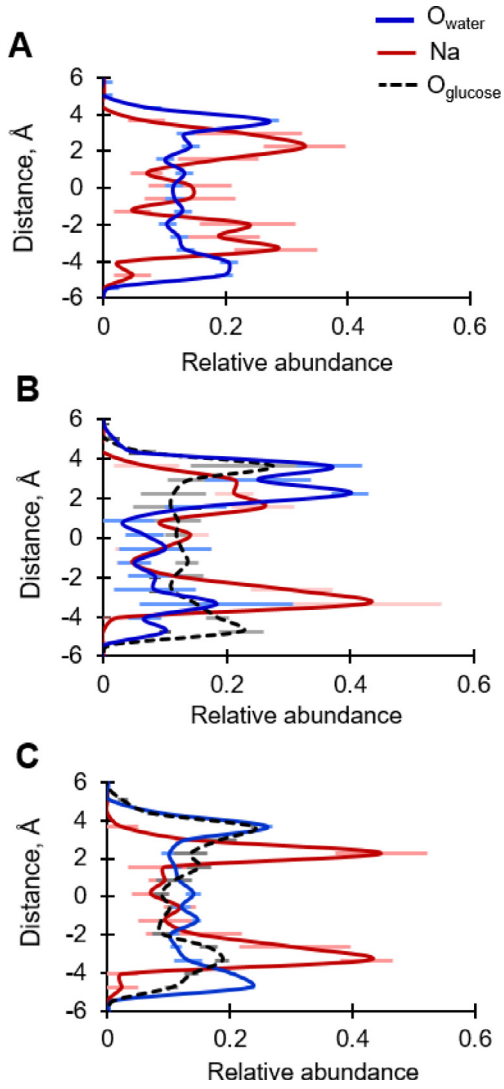

Fig. 2. Dynamic interlayer density profile (average ± standard error) of water O atoms (blue line), Na (dark red line), and glucose O atoms (dotted black line) in the absence of glucose (A) and in the presence of 0.5 mM glucose concentration (B) or 2 mM glucose concentration (C). Plots show as averaged valued with error bars representing standard deviation of data obtained from a 10 ns-MD production run at 1-ns time intervals.

nal to the mineral surface and multiple very low-abundance peaks for the water molecules away from the mineral surface (Fig. 2A). However, within the imprecision of the fluctuating motions of the atoms throughout the MD run, the water density profile obtained in the high-glucose interlayer was similar to that in the no-glucose nanopore (Fig. 2A and C). Thus, at first glance, organization of the water molecules alone could not account for the significant decrease in the D_{water} in the high-glucose interlayer when compared to the no-glucose interlayer (Table 1; Fig. 2A and C).

On the other hand, changes in the interlayer organization of the Na ions provided clues into the spatial re-organization responsible for the changes in both D_{water} and D_{Na} as a function of glucose content in the nanopore. In the absence of glucose, the two high-abundance populations of Na ions near the surface were represented by broad peaks (Fig. 2A). In the low-glucose interlayer, the Na density profile reflected both a broad peak at one interfacial region and a narrower peak at the opposite interfacial region (Fig. 2B). Also, in the high-glucose nanopore, two narrow Na density peaks occurred near the mineral surface at greater relative abundance than in the two aforementioned nanopore systems without glucose or with relatively lower glucose content (Fig. 2C). Specifically, there was a near 50% increase in the relative abundance of Na ions near the mineral interface in the high-glucose interlayer (Fig. 2A and C). Previous MD simulations with Na-montmorillonite have reported that the first monolayer of Na ions at the mineral interface exhibited 4 to 20 times lower D values than the Na ions in bulk solution (Bourg and Sposito, 2011). Therefore, re-organization of Na_+ ions in the interlayer nanopore explained the significant decrease in D_{Na} with increasing glucose concentrations in our simulated systems (Table 1 and Fig. 2). The hydration shell associated with Na ions accumulated at the mineral interface in the high-glucose nanopore would result in a relatively higher amount of water molecules localized at the mineral surface than in the no-glucose nanopore (Marry et al., 2008; Botan et al., 2011). We propose that these Na-solvated water molecules near the mineral surface are less subjected to molecular exchanges with other water populations away from the mineral interfacial regions, thus resulting in significant reduction in D_{water} in the high-glucose nanopore (Table 1). In accordance with this proposal, the layer of water molecules closest to the montmorillonite and other mineral surfaces was reported to have the lowest D_{water}, when compared with bulk water or mid-plane interlayer water (Bourg and Sposito, 2011).

In terms of the interlayer organization of glucose, there were three notable observations. First, the density profile of the glucose O atoms peaked near the mineral surface (Fig. 2B and C). Second, there were more fluctuations in the glucose density profile in the low-glucose nanopore than in the high-glucose nanopore Fig. 2B and C). Third, a slight decrease in the peak abundance of glucose O atoms near the mineral surface in the high-glucose nanopore was accompanied by a broadening of the peak with distance away from the surface (Fig. 2B and C). These observations implied that the molecular movement of glucose compounds were less dynamic with increasing glucose concentrations due to promoted interactions of the glucose compounds at the mineral surface and aggregation of these compounds into clusters as the glucose content increased (Fig. 2). These changes in the interlayer organization explained the significant reduction in $D_{glucose}$ as the glucose concentration was increased 4 times (Table 1).

3.3. Radial distribution functions and coordination

We investigated further the coordinated structural arrangement of adsorptives with respect to each other and to the montmorillonite surface via RDFs (Figs. 3 and 4). Fig. 3 illustrates the RDFs and CN values for water-water, water-clay, Na-water, and Na-clay and Na-clay intermolecular arrangements, and Fig. 4 illustrates the corresponding values for the intermolecular arrangements of glucose-water and glucose-clay coordination.

The arrangement of water molecules with respect to each other and the mineral surface remained mainly unchanged as the pore volume became more filled with glucose compounds (Fig. 3A–D). The H_{water}-O_{clay} RDFs indicated that the water molecules close to the mineral surface occupy more variable positions in the high-glucose nanopore than in the low-glucose or no-glucose interlayer (Fig. 3C and D). This dynamic behavior may be due to the decreased amount of water-water interactions needed to stabilize the clay-water interactions in the high-glucose nanopore (SI, Appendix B; see also later discussion on water-water H-bonding interactions). However, the computed CN from these RDFs did not show any change in the coordination of O_{water} close to the mineral surface (Fig. 3B). The RDF curves for H_{water} –O_{water} have similar characteristic shapes for all three simulated systems (Fig. 3A). First, there was a sharp peak at 0.93–1.03 Å, which can be attributed to both closely coordinated O_{water} and self-pairing O_{water} coordination (i.e. the presence of O_{water} in the same molecule that contains the reference H_{water}). A second smaller peak was captured for a

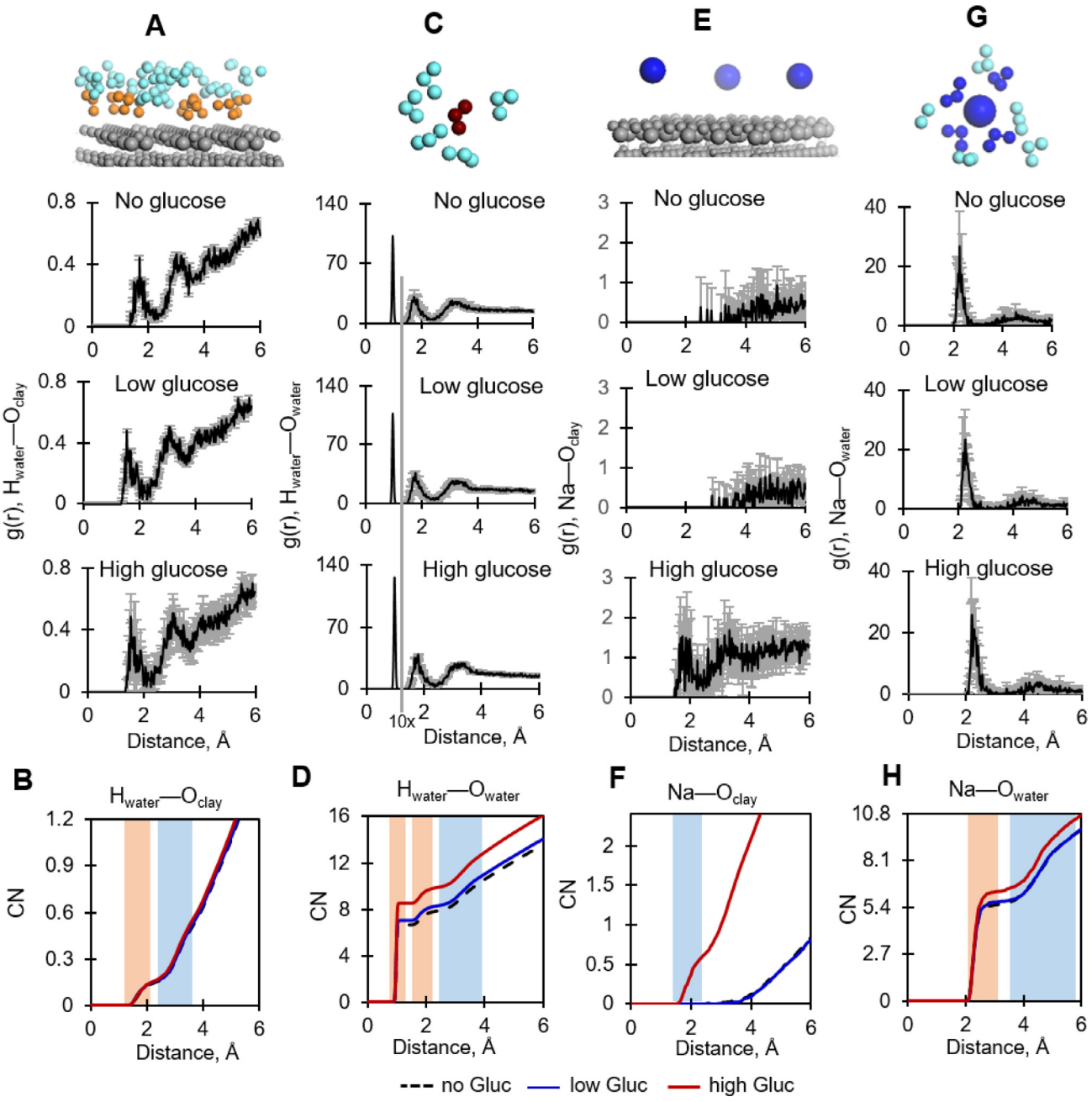

Fig. 3. Dynamic radial distribution function [RDF, $g(r)$] of water H and clay O (H_{water}—O_{clay}) (A), water H and water O (H_{water}—O_{water}) (C), Na and clay O (Na—O_{clay}) (E), and Na and water O (Na—O_{water}) (G) and computed coordination values (CN) for H_{water}—O_{clay} (B), H_{water}—O_{water} (D), (Na—O_{clay}) (F), and (Na—O_{water}) (H). In A, C, E, and G, the top picture illustrates the structural environment being monitored and the RDFs for the nanopores with no glucose, low glucose (0.5 mM), and high glucose (2 mM) concentration are shown, respectively, from top to bottom; the RDF data obtained over the course of the MD production run (10 ns) are shown as time-averaged values, with error bars representing the standard deviation. In B, D, F, and G. the CN values for the no-glucose, low-glucose, and high-glucose nanopores are shown, respectively, in black dotted line (no Gluc), blue line (low Gluc), and red line (high Gluc); the shaded orange and blue areas indicate well–defined and diffuse coordination shells, respectively. For clarity, only the average CN values are plotted. The first peak in the H_{water}—O_{water} RDFs (Panel C) include self-pairing between O and H atoms within the same water molecule as well as closely-coordinated atoms. Compared to the CN profile for the no-glucose and low-glucose nanopores, the difference in the CN profile determined for Na—O_{clay} in the high-glucose nanopore was statistically-significant ($p \leq 0.05$).

statistical layer of O_{water} occurring at a radial distance of 1.50–2.40 Å from the reference H_{water} (Fig. 3A). A third peak illustrated a not-well-defined H_{water}-O_{water} coordination occurring at a radial distance of 2.40–3.90 Å (Fig. 3A). The CN values obtained from integrating the RDFS of H_{water}-O_{water} shed light on the amounts of molecules in each coordination shell (Fig. 3B). The coordination environment of a water molecule with respect to other water molecules in the low-glucose nanopore remained relatively unchanged compared to the nanopore with no glucose (Fig. 2B). In contrast, the average CN values of O_{water} coordinating H_{water} in the high-glucose nanopore indicated an additional O_{water} atom in the first coordination shell but these values were not statistically significant when taking into account the standard deviation of the RDF profiles (Fig. 3D).

With respect to coordination of Na_+ ions at the mineral basal surface, the Na—O_{clay} RDFs showed the appearance of a peak at a radial distance of 1.49–2.5 Å in the high-glucose nanopore, which did not occur in the other two simulated systems (Fig. 3E). The for-

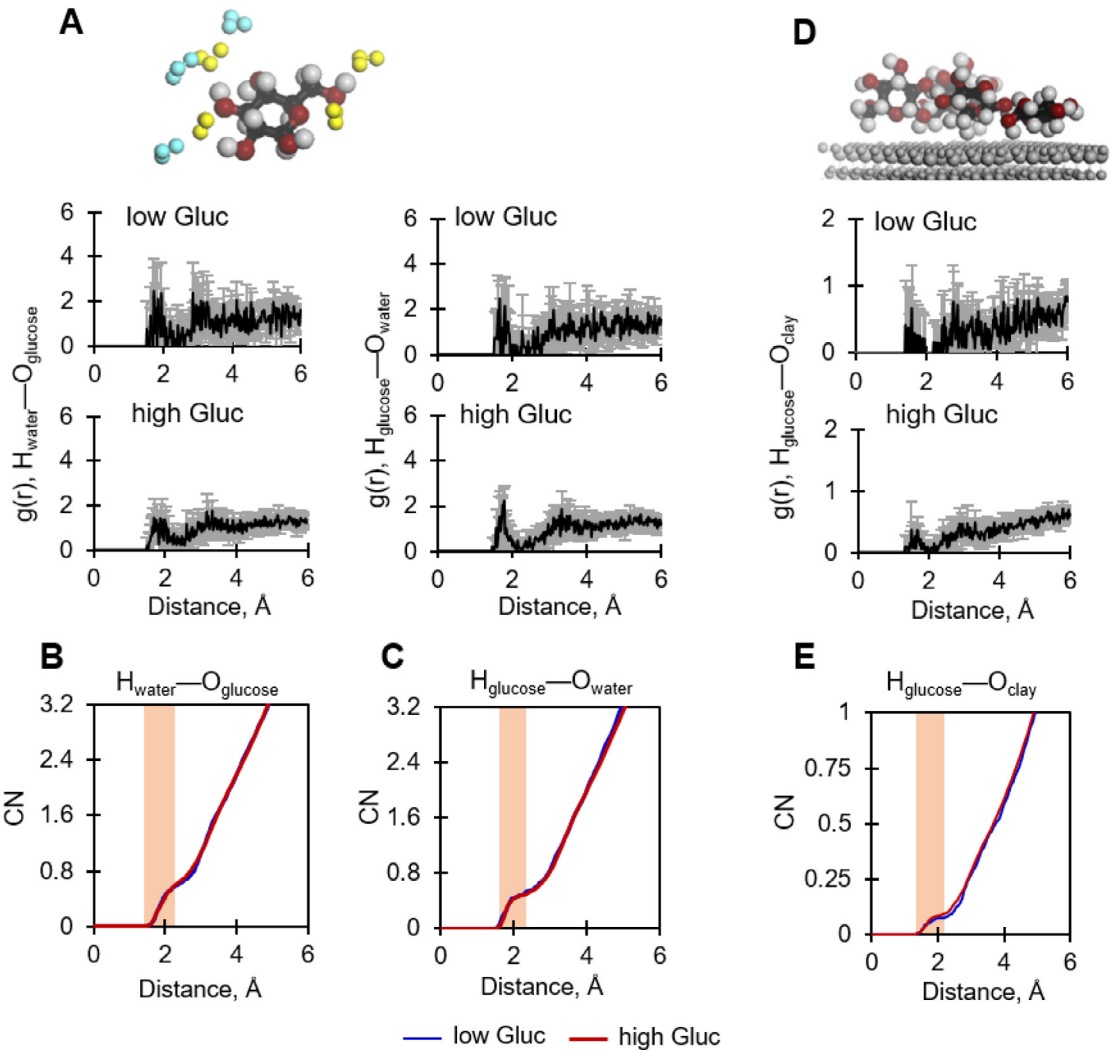

Fig. 4. Dynamic radial distribution function [RDF, $g(r)$] of water H and glucose O (H_{water}—$O_{glucose}$) (A, left), glucose H and water O ($H_{glucose}$—O_{water}) (A, right), glucose H and clay O ($H_{glucose}$—O_{clay}) (D); and, computed coordination values for H_{water}—$O_{glucose}$ (B), O_{water}—$H_{glucose}$ (C), $H_{glucose}$—O_{water} (E). In A and C, the top picture illustrates the structural environment being monitored and the RDFs for the nanopores with low glucose (0.5 mM) and high glucose (2 mM) concentration are shown, respectively, on top and bottom; the RDF data obtained over the course of the MD production run (10 ns) are shown as time-averaged values, with error bars representing standard deviation. In B, C, and E, the CN values are shown for the low-glucose and high-glucose nanopores in blue line (low Gluc), and red line (high Gluc), respectively—for clarity, only the average CN values are plotted; the shaded orange and blue areas indicate well–defined and diffuse coordination shells, respectively.

mation of this coordination shell was highly variable as indicated by the high standard deviation values of the RDF curve (Fig. 3E). However, it was clear that this statistical layer of O_{clay} close to Na ions was absent in the nanopore with 4 times lower glucose concentration or without any glucose (Fig. 3E). The CN values computed from the Na—O_{clay} RDFs further demonstrated a layer of inner-sphere Na complexes close to the mineral surface in the high-glucose nanopore (Fig. 3F). These results are consistent with the adsorptive density profile illustrated in Fig. 2 wherein the Na density profile in the high-glucose nanopore exhibited the higher-abundance and narrower density peaks near the mineral surface than the Na density profiles in the no-glucose and low-glucose nanopores, which indicated lower abundance values and broader peaks.

The characteristic shape of the Na-O_{water} RDFs was the same for all three simulated nanopores with a well-defined coordination shell captured at 2.0–3.0 Å and a relatively more diffuse coordination shell at 3.7–6.0 Å (Fig. 3G). The computed CN values from the Na-O_{water} RDFs indicated that, on average, the high-glucose nanopore had greater amount of Na-solvated water molecules, about 0.5 to 0.7 more, than the coordination environments in the nanopore without glucose or with low glucose (Fig. 3H). Although this difference was not statistically significant given the fluctuations in the RDF profiles over the course of the entire MD run, it suggested higher occurrences of the solvation shell of Na ions with higher amount of solvated waters when glucose compounds occupied a relatively high amount of the nanopore volume (Fig. 3E and F). This phenomenon would be promoted by the aforementioned presence of inner-sphere Na complexes at the mineral surface in the high-glucose nanopore.

We also investigated the coordination of water molecules relative to the glucose compounds by obtaining both H_{water}—$O_{glucose}$ and $H_{glucose}$—O_{water} RDFs in the glucose-containing interlayer nanopores (Fig. 4A). Overall, both sets of RDFs indicated similar profiles but it was clear that the RDFs obtained with the high-glucose interlayer were more defined and exhibited much less fluctuation around the time-averaged data (Fig. 4A). The corresponding CN profiles also indicated that the glucose-water structural arrangement was similar in both interlayer nanopores, with a water coordination shell within 1.49–2.55 Å radial distance from the glucose (Fig. 4B and C). In terms of arrangements of glucose relative to the mineral surface as captured by $H_{glucose}$—O_{clay} RDFs, we

Table 2
Molecular dynamics (MD)-optimized networks of hydrogen bonds (H-bonds) in the montmorillonite interlayers[a].

	Glucose concentration in the mineral nanopore		
	0	0.5 mM	2 mM
Water-water H-bonds[b]	353 ± 0	361 ± 1	327 ± 2
Water-clay H-bonds[b]	84 ± 6	88 ± 4	92 ± 2
Water-glucose H-bonds[b]	–	20 ± 8	78 ± 2
Glucose-clay H-bonds	–	3 ± 2	15 ± 3
Glucose-glucose H-bonds	–	1 ± 1	12 ± 3

[a] MD production run was conducted for 10 ns, following a 1 ns MD pre-equilibration step, at 298 K. The MD data are reported as average ± standard deviation.
[b] Normalized by the water content in the nanopore

also obtained similar coordination environments in both interlayer nanopores but less variable RDFs in the high-glucose nanopore than in the low-glucose nanopore (Fig. 4D and E). These results implied reduced motions of glucose molecules at the mineral interfacial region as the pore volume became more populated with the organic compounds, which in turn explained the reduction in $D_{glucose}$ in the high-glucose nanopore compared to the low-glucose nanopore.

3.4. Network of hydrogen bonding interactions

Our results presented thus far implied that an increase in Na coordination and its associated water molecules at the mineral interface led to the decrease in D_{water} and D_{Na} in the glucose-populated nanopores compared to the no-glucose nanopore. In addition, the reduction in $D_{glucose}$ with increasing glucose concentration in the montmorillonite interlayer space can be attributed in part to intermolecular interactions between clustered glucose compounds at the mineral surface. It is important to note that coordination environments captured in RDFs do not necessarily translate into favorable H-bonding interactions. We determined how networks of the following intermolecular H-bonds changed in the interlayer nanopore in response to added glucose compounds: water-water H-bonds, water-clay H-bonds, glucose-water H-bonds, glucose-clay H-bonds, and glucose-glucose H-bonds (Table 2).

The interactions of the water molecules with the mineral surface via H-bonds remained unchanged in the presence of the two glucose populations (Table 2). When the glucose content was increased by a factor of 4 in the clay nanopore, there was a near 10% decrease in water-water H-bonds accompanied by a near four-fold increase in water-glucose H-bonds (Table 2). Thus, an increase in water-glucose H-bonds seemed to be correlated with an altered water-water structure resulting in a reduced amount of water-water H-bonds (Table 2). Therefore, in addition to the interfacial immobilization of Na-associated waters discussed above, the disruption of favorable water-water interactions by glucose-captured waters may have also contributed to the decrease in D_{water} in the high-glucose nanopore.

The amount of glucose-clay H-bonds and glucose-glucose H-bonds supported the conclusions made from the data obtained from the density profiles and the RDFs (Figs. 2 and 3; Table 2). Specifically, a significant increase in glucose-glucose H-bonds was in accordance with both the decreased fluctuations in the glucose density profile and the aggregation of glucose compounds implied by the interlayer profile of glucose O atoms (Fig. 2). Also, a five-fold increase in glucose-clay H-bonding interactions as glucose content increased was in agreement with both the reduced dynamics in glucose-clay RDF profiles and the reduction in D_{water} (Table 1, Table 2, Fig. 4D).

3.5. Re-organization of water molecules in glucose-containing nanopores

The different changes in chemical interactions and their subsequent implications on the molecular diffusion in the montmorillonite interlayer nanopores are reflected in the structural re-organization of water molecules within the nanopore (Fig. 5). Using MD snapshots of the three simulated conditions, Fig. 5 illustrates the four populations of water adsorbate species as defined by their involvement in H-bonding hydrating interactions and cation solvation shell: 1. Water molecules involved in water-water interactions (light blue), 2. Water molecules involved in solvating the Na ions in the first hydration shell (dark blue), 3. Water molecules involved in hydrating the clay surface via direct H-bonds (orange), and 4. Water molecules involved in hydrating glucose via direct H-bonds (yellow). The increased occupation of the nanopore volume by the glucose compounds resulted in patchiness in the water-water interactions (Fig. 5). Water molecules that are within the first hydration shell of Na were seldom found simultaneously at the mineral interface in the absence of glucose (Fig. 5A). However, as more glucose was introduced in the interlayer of the nanopore, water molecules in the Na hydration shell and those interacting directly with the mineral were occurring more at the same spatial location within the nanopore (Fig. 5). Water molecules interacting with glucose were dispersed at low-glucose content but, in the high-glucose nanopore, glucose-hydrated waters were coalescing as they form a cage around the aggregated glucose molecules (Fig. 5).

3.6. Sugar-Influenced ^{23}Na NMR and XRD of Na-Montmorillonite

We obtained solid-state ^{23}Na NMR data of the montmorillonite samples without and with intercalated glucose (Fig. 6). A previous ^{23}Na NMR study of saponite, a smectite-type clay, proposed a decrease in signal intensity due to fast exchange in Na^+ (Grandjean, 2001). A strong interaction of the metal cation at the mineral surface was reported to reduce this exchange rate and thus should result in an increase in the ^{23}Na NMR intensity (Grandjean, 2001). Our ^{23}Na NMR spectra revealed two distinct signal populations of Na (Fig. 6). One signal was characterized by a broad small peak in the no-glucose sample (Fig. 6A). We attributed this signal to a small population of outer-sphere Na ions that remained present specifically in Na-enriched montmorillonite, even after the freeze-drying step (Fig. 6A). This signal persisted as a barely visible signal on the right side of the main central peak in the glucose-enriched samples (Fig. 6A–D). The second signal was characterized by a sharp central peak and its intensity was increased proportionally with the increasing glucose concentrations in the reacted mixture (Fig. 6B–D). This second Na population thus indicated a decrease in exchange rate of Na_+ as the glucose content increased, in accordance with our theoretical predictions of glucose-induced immobilization of Na on the mineral surface. It was not possible to deduce from these NMR results the exact localization of this second population, edge surface sites versus basal sites.

The XRD measurements of Na-montmorillonite with an increasing amount of glucose content at different RH conditions provided qualitative examination of the theoretical predictions of glucose-influenced water behavior in the nanopores (Fig. 7). At the highest recorded RH (90%), all four different scenarios (montmorillonite reacted with no glucose or with three different glucose concentrations) exhibited about the same d_{001}, ~1.55–1.56 nm (Fig. 7). As pointed out in the Introduction, this range of d_{001} corresponds to bi-hydrated Na-saturated montmorillonite interlayers (Ferrage, 2016). The corresponding FWHM values fell within a narrow range, 0.41 to 0.45 2θ, thus indicating similar interstratified layer types

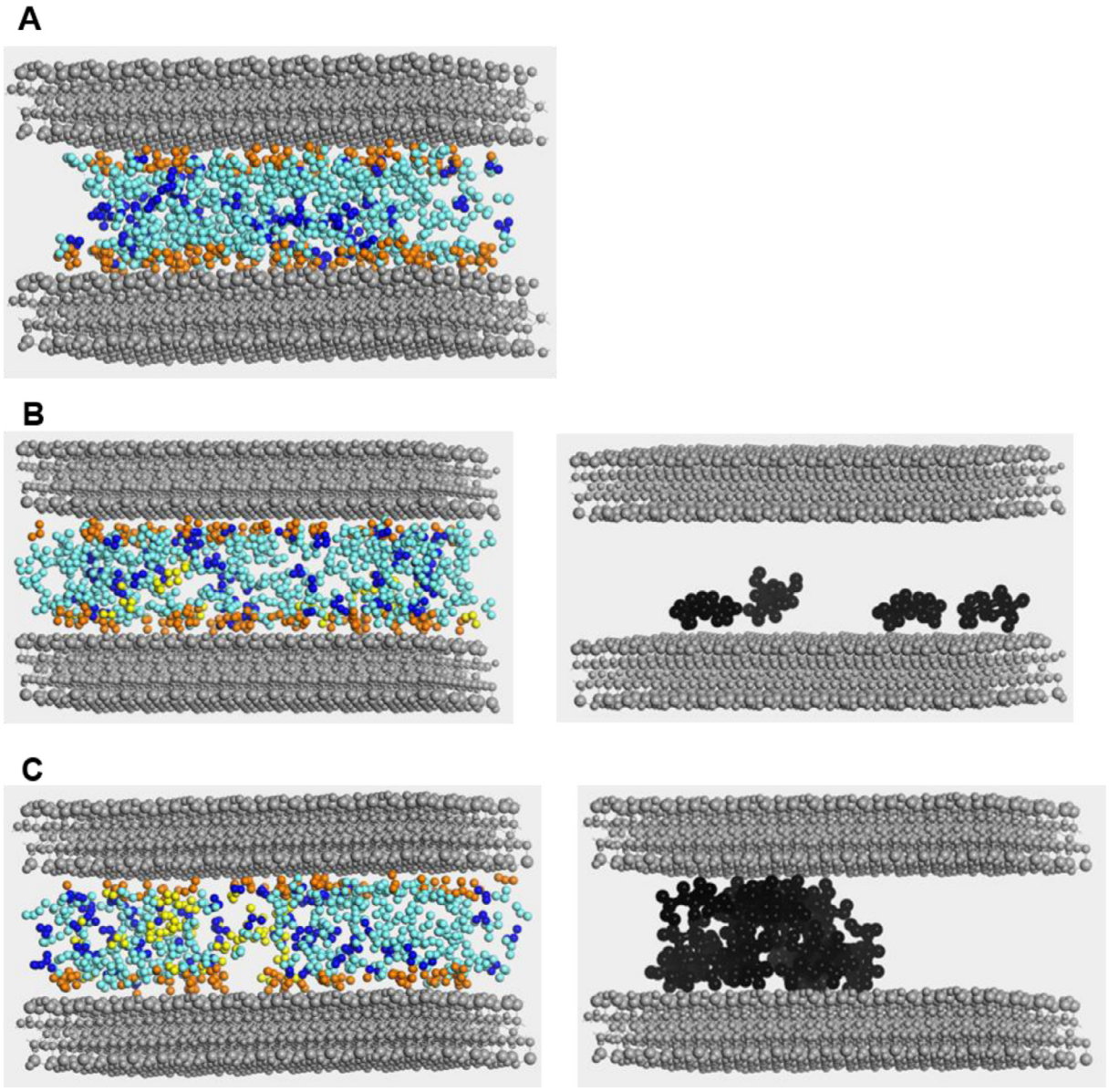

Fig. 5. Water populations in a snapshot of the molecular dynamics-optimized hydrated montmorillonite nanopores populated with no glucose (A), 4 glucose molecules (B), and 16 glucose molecules (C). In B and C, the interlayer with the water molecules alone and the glucose molecules alone are shown, respectively, on the left and on the right. Color legend: Na-solvating waters in the first hydration shell (dark blue), water hydrating the clay surface via direct H-bonds (in orange), and water H-bonded with glucose molecules (in yellow); glucose molecules (black). (For interpretation of the references to colour in this figure legend, the reader is referred to the web version of this article.)

regardless of the glucose content at 90% RH (Fig. 7). Because this FWHM range at 90% RH represented the smallest FWHM values recorded from all the XRD data, we concluded that the interstratification was the most homogenous at high RH, likely due to the same extent of enrichment of the nanopores with water molecules (Ferrage et al., 2005). A decrease in the RH condition from 90% to 50% led to a 0.35 nm decrease in the d_{001} of the no-glucose interlayer, but the d_{001} with the glucose-populated interlayers was only decreased by 0.13 nm to 0.19 nm (Fig. 7). The corresponding FWHM values, which reflect the broadening of the 001 peaks, indicated that the heterogeneity of the interstratified interlayers was quite different under the different glucose scenarios at 50% RH (Fig. 7). At 50% RH, compared to the FWHM of 0.87 2θ for the no-glucose interlayer, the FWHM for the low-glucose interlayers (0.5 mM and 2 mM) was 1.53 and 1.41 2θ respectively and the FWHM for the high-glucose (20 mM) interlayer was 0.409 2θ (Fig. 7). Therefore, at 50% RH, the least heterogeneous interstratification was recorded in the absence of glucose or in the presence of high-glucose populated nanopores. The relatively larger FWHM values obtained at lower glucose content reflected XRD signatures between the two end-members, no-glucose versus glucose-saturated nanopores (Fig. 6).

The XRD profiles conducted at the low hydration of 20% RH were previously used to capture the optimal contrast of the d_{001} of Na-montmorillonite with and without intercalated organic molecules (Aristilde et al., 2010; Aristilde et al., 2013; Aristilde et al., 2016). Here the XRD data recorded at 20% RH revealed clear evidence of intercalated glucose within the Na-montmorillonite layers (Fig. 7). The d_{001} for Na-montmorillonite in the absence of glucose at 20% RH was 1.16 nm (Fig. 7). However, the corresponding d_{001} of the Na-montmorillonite reacted with 0.5 mM, 2 mM, and 20 mM glucose, was respectively 1.22 nm, 1.22 nm, and 1.41 nm (Fig. 7). At the 20% RH, the FWHM value for the interlayer in the absence of glucose was 0.964 2θ but was increased to 1.22

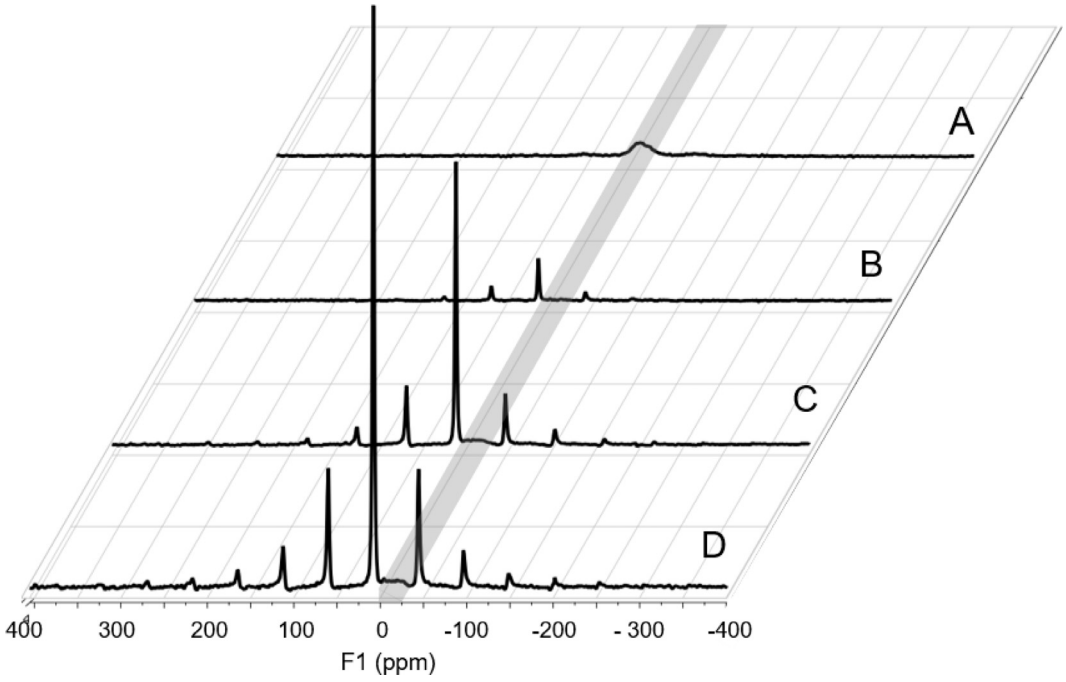

Fig. 6. Solid-state ^{23}Na NMR data of glucose-montmorillonite samples following reactions with glucose solutions at 0 mM (A), 0.5 mM (B), 2 mM (C), and 20 mM (D). The shaded area shows the localization of the specific signal found in the absence of glucose in the sample.

2θ with 0.5 mM glucose, 1.65 2θ with 0.2 mM glucose, and decreased to 0.40 2θ with 20 mM glucose (Fig. 7). The relatively higher heterogeneity of the lower-glucose interlayers (reacted with 0.5 mM and 2 mM glucose) than the high-glucose interlayer (reacted with 20 mM glucose) reflected different layer types in the lower-glucose interstratified layers that would include both no-glucose interlayers as well as glucose-containing interlayers. A similar phenomenon was reported for the evolution of interstratified interlayers as a function of increasing amount of adsorbed antibiotic compounds at 20% RH (Aristilde et al., 2013).

In sum, the moisture-dependent XRD profiles showed changes in d_{001} and FWHM values that were dependent on the glucose content (Fig. 7). In the absence of glucose, the XRD data indicated that the d_{001} values at 20% RH (1.16 nm) and 50% RH (1.2 nm) were close to the minimum d_{001} (1.18 nm) assigned to mono-hydrated layers (Ferrage et al., 2005). On the other hand, the d_{001} value at 90% RH (1.55 nm) for the glucose-free interlayer was near the maximum d_{001} set for bi-hydrated interlayers (1.58 nm). This explains the difference in the FWHM values, which indicated that the interstratified interlayers at 90% RH in the absence of glucose were less heterogeneous than at the lower RH conditions. Whereas the collapse of the d_{001} of the glucose-free montmorillonite interlayers was by 0.40 nm from the 90% RH to 20% RH conditions, the corresponding d_{001} collapse for the glucose containing interlayers was 0.33 nm, 0.34 nm, and 0.01 nm following, respectively, reaction of montmorillonite with 0.5 mM, 2 mM, and 20 mM glucose (Fig. 7). Therefore, glucose-enriched montmorillonite nanopores were resistant to interlayer collapse in response to dehydrating conditions (Fig 6). Accordingly, the FWHM values indicated that populations of interstratified layers with higher hydration states are maintained in the glucose-containing nanopores more than in the no-glucose interstratified layers (Fig. 7).

4. Discussion

In the Introduction, building on findings from previous MD simulations, we put forth four hypotheses of how glucose presence in montmorillonite nanopores may interfere with the fluid-mineral interfacial interactions and subsequently alter the diffusion of water molecules and solutes. The first hypothesis was that Na diffusion would be altered by glucose-mediated changes in the localization of Na adsorptive species. We found that both D_{water} and D_{Na} were decreased in glucose-containing nanopores compared to the glucose-free nanopores and this decrease was more pronounced in the high-glucose nanopore (Table 1). A previous MD study on the effects of water content on the adsorption of Na^+ ions indicated that Na adsorptive species changed from outer-sphere complexes to inner-sphere complexes as water content decreased (Zhang et al., 2014). From their MD results, Sutton and Sposito (2006) reported that a large polar organic polymer model can dehydrate the solvation shell of cations, further facilitating the inner-sphere complexation of the cations in the presence of the organics. The increase in the glucose content in our simulated nanopore necessitated a decrease in the water content in our simulated nanopores (SI, Appendix B). Accordingly, the Na coordination environment, as deduced from the RDF profiles indicated inner-sphere complexes of Na ion in the high-glucose, which were absent in the low-glucose and no-glucose montmorillonite nanopores (Fig. 3H).

In support of the simulation results, the solid-state ^{23}NMR experimental examinations provided strong evidence that glucose affected the interactions of Na ions with the montmorillonite surface (Fig. 6). The ^{23}NMR results revealed a population of Na in the presence of glucose that was distinct from the indigenous Na ions in the Na-enriched montmorillonite in the absence of glucose (Fig. 6). We attributed this new Na population to the accumulated Na ions at the mineral surface via inner-sphere complexation predicted by the MD findings.

The second hypothesis was that the changes in the water diffusion are due to changes in the water hydration at the mineral interface. Previous MD reports have found that the slower diffusion of water at the mineral interface can be attributed to longer residence time of both water molecules H-bonded to O atoms of the siloxane basal surface in montmorillonite and those involved in the hydration shell of interlayer cations (Botan et al., 2011; Marry et al., 2008; Lee et al., 2013). The amount of water-clay H-bonds remained unchanged in the presence of both populations of glucose,

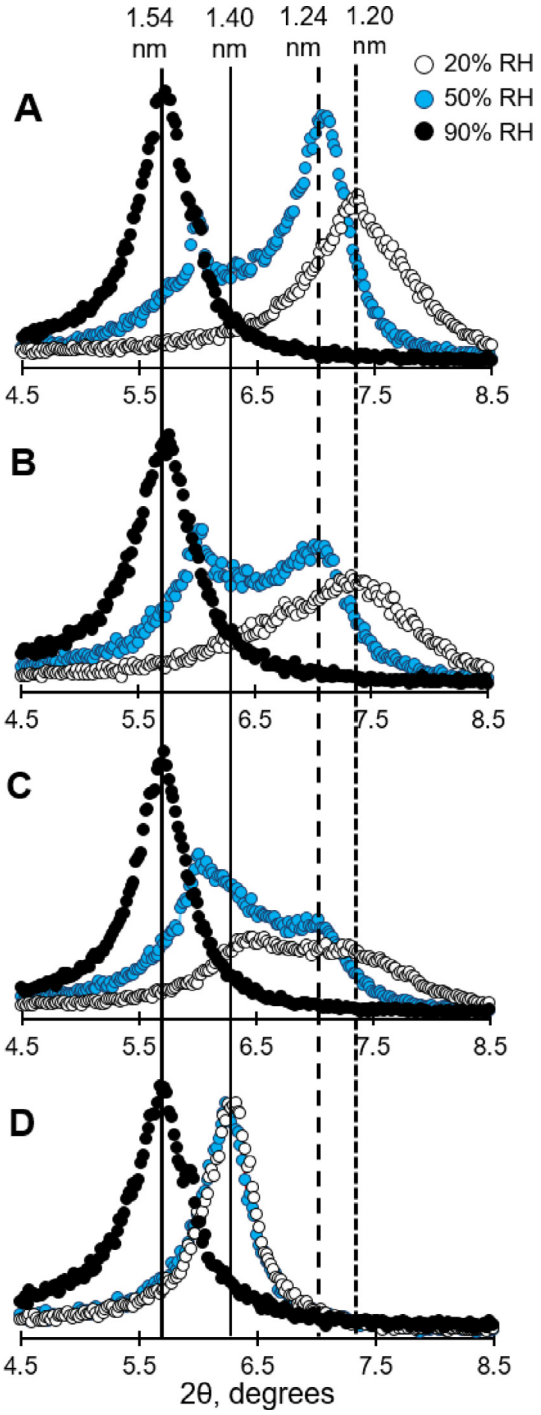

Fig. 7. X-ray diffraction patterns of montmorillonite layers in the absence of glucose and following reactions with glucose solutions at different concentrations: 0 mM (A), 0.5 mM (B), 2 mM (C), and 20 mM (D). The oriented clay layers were equilibrated at different relative humidity (RH) conditions: 90% (black symbols), 50% (light blue symbols), and 20% (white symbols). The 2θ-degree values for d_{001} of 1.54, 1.40, 1.24, and 1.20 nm are indicated, respectively, by a thick line, a thin line, a long-dash line, and a short-dash line. (For interpretation of the references to colour in this figure legend, the reader is referred to the web version of this article.)

compared to the nanopore without any glucose (Table 2). However, in the high-glucose nanopore, our atomistic density profiles showed that there was greater accumulation of Na^+ ions at the mineral interface (Fig. 2C). The latter phenomenon would lead to higher population of water molecules at the fluid-mineral interface in the high-glucose nanopore, in support of the second hypothesis.

The third hypothesis was that water-water interactions are disrupted by the presence of glucose. We found that, in addition to the increased occupied nanopore volume by glucose, H-bonding interactions between water molecules and the glucose molecules decreased the population of waters involved in both the solvation of Na ion ions and the water-water structure (Fig. 5). With regards to the widely used electrical double layer model as the structural framework for water and solute arrangement on mineral surfaces (Bourg and Sposito, 2010; Sposito, 2004; Tournassat et al., 2009), our results demonstrated that the presence of small uncharged polar organic molecules such as glucose imposed a disorder in the interlayer organization of water molecules and cations and enhanced the population of inner-sphere adsorbate ion species, both of which are less pronounced in the absence of glucose.

The fourth hypothesis posited that the mobility of glucose would be reduced due to interactions with the mineral surface. Previous DFT (Lee et al., 2013) and MD (Sutton and Sposito, 2006) simulations have reported that glucose and other polar organic molecules participated in H-bonding interactions with the siloxane basal surface of montmorillonite. We found that a 75% decrease in $D_{glucose}$ was accompanied by a 5-fold increase in glucose-clay H-bonds (Tables 1 and 2). A MD study of glucose aqueous solutions reported an increase in both glucose-glucose H-bonding interactions as the concentration of glucose increased (Chen et al., 2012). Here we also found that glucose-glucose H-bonds facilitated clustering of glucose molecules into aggregates in the high-glucose nanopore (Table 2; Fig. 5C). Such aggregates were shown to induce facilitated diffusion in MD-simulated alkyl hydrocarbons within montmorillonite nanopores (Zhang et al., 2016). In the case of our high-glucose system wherein glucose participated in both intramolecular H-bonds within glucose-glucose flocs and intermolecular H-bonds with the mineral surface, the aggregation of glucose molecules resulted instead in promoted immobilization of glucose in the nanopore.

Our XRD measurements revealed interlayer properties that were in qualitative agreement with our MD-predicted results. As was recently reported with the sugar dimer lactose (Hellrup et al., 2016), our XRD data also indicated intercalation of glucose in the montmorillonite interlayers (Fig. 7). The MD results revealed aggregated clusters formed by the glucose molecules in which multiple H-bonds held the organic clusters to each other and to the clay basal surface on both walls of the nanopore. In accordance with this MD-predicted interlayer organization of the glucose molecules, the XRD data demonstrated that glucose-rich montmorillonite interlayers were resistant to shrinking upon reducing moisture conditions. Specifically, the collapse of the glucose-rich interlayers revealed by the XRD data in response to reducing moisture conditions was only 2.5% of the collapse undergone by the glucose-free interlayers (Fig. 7). Also, consistent with the slowed molecular diffusion of water in glucose-populated nanopores, the XRD profiles indicated that these glucose-enriched nanopores tend to maintain layer types with higher hydration states than the no-glucose nanopores.

5. Conclusion

Plant secretions of sugars and sugar-containing polymers enhance water-holding capacity of soils near the root zone (Carminati et al., 2011; Paynel et al., 2013; Ahmed et al., 2014). The present study aimed to gain insights on the influence of chemical interactions on the molecular diffusion within sugar-containing fluids trapped within smectite-type clay mineral nanopores. Glucose-captured water molecules contributed to the depletion of solvated waters around Na ions. Compared to the nanopores without glucose, the MD simulations revealed that Na^+ ions were more tightly associated with the mineral surface via inner-sphere complexes in

the high-glucose interlayer nanopore, thus resulting in slowed diffusion of both Na and its remaining hydrated waters. Experimental ^{23}Na NMR measurements confirmed the evolution of immobilized Na^+ ions at the mineral interface as a function of increasing glucose content. The reduced mobility of glucose as a function of increasing glucose content in the nanopore was due to an increase in both glucose-glucose interactions and glucose-clay interactions. The theoretical predictions of reduced mobility of both water molecules and solutes in glucose-enriched molecules were corroborated by experimental moisture-dependent XRD analyses of glucose-montmorillonite composites at varying glucose content.

In the broader context of the relationship between sugars and soil moisture in the vadose zone, our findings provide insights into the mechanisms through which sugars in clay nanopore fluids promote the trapping of both water and metal nutrients within soils. Of crucial importance to the management of soil water retention in drought-prone soils are the implications of our findings for the role of this trapped water in maintaining inaccessible soil moisture versus sustaining potentially plant-available soil water (Sposito, 2013). Deciphering these implications represents important next steps for further investigation of the role of sugars and relating molecules in influencing hydrodynamics within nanopores, micropores, and macropores of soils.

Acknowledgments

This work made use of the Cornell University NMR facility (Department of Chemistry and Chemical Biology), which is supported in part by a NSF-MRI grant (CHE-1531632). We are very grateful to Ivan Keresztes and the rest of the Cornell University NMR facility for assistance with the NMR measurements and analyses. Both the X-ray diffraction measurements and undergraduate research support for S.M.G and T.G.A. were facilitated by a grant for instrument upgrade and research outreach provided by the U.S. National Science Foundation Division of Earth Sciences (EAR-IR 1343063). Graduate support for S.E.K. was through an Integrative Graduate Education and Research Traineeship (IGERT) research fellowship from the U.S. National Science Foundation. This work was also supported in part by a start-up package from Cornell University. In light of this special issue honoring Dr Garrison Sposito in occasion of his retirement, L.A. (currently a faculty in the Department of Biological and Environmental Engineering at Cornell University) dedicates this paper to Dr Sposito and thanks him for encouraging her to pursue her scientific curiosity, both during and after her tenure as his doctoral student (2003–2008) at the University of California-Berkeley.

Supplementary materials

Supplementary material associated with this article can be found, in the online version, at doi:10.1016/j.advwatres.2017.03.014.

References

Accelrys Software Inc, 2013. Discovery Studio Modeling Environment. Accelrys Software Inc., San Diego.
Ahmed, M.A., Kroener, E., Holz, M., Zaerbanadkouki, M., Carminati, A., 2014. Mucilage exudation facilitates root water uptake in dry soils. Func. Plant Biol. 41, 1129–1137.
Allen, M.P., Tildesley, D.J., 1987. Computer Simulation of Liquids. Clarendon Press, Oxford, pp. 182–208.
Aristilde, L., Sposito, G., 2008. Molecular modeling of metal complexation by a fluoroquinolone antibiotic. Environ. Toxicol. Chem. 27, 2304–2310.
Aristilde, L, Marichal, C, Miéhé-Brendlé, J., Lanson, B., Charlet, L., 2010. Interactions of oxytetracycline with a smectite clay: a spectroscopic study with molecular simulations. Environ. Sci. Technol. 44, 7839–7845.
Aristilde, L., Sposito, G., 2010. Binding of ciprofloxacin by humic substances: a molecular dynamics study. Environ. Toxicol. Chem. 29, 90–98.
Aristilde, L., Lanson, B., Charlet, L., 2013. Interstratification patterns from the pH-dependent intercalation of a tetracycline antibiotic within montmorillonite layers. Langmuir 29, 4452–4501.
Aristilde, L., Lanson, B., Miéhé-Brendlé, J., Marichal, C., Charlet, L., 2016. Enhanced interlayer trapping of a tetracycline antibiotic within montmorillonite layers in the presence of Ca and Mg. J. Coll. Interf. Sci. 464, 153–159 2016.
Berendsen, H.J.C., Grigera, J.R., Straatsma, T.P., 1987. The missing term in effect pair potentials. J. Phys. Chem. 91, 6269–6271.
Blunt, M.J., Bijeljic, B., Dong, H., Gharbi, O., Iglauer, S., Mostaghimi, P., Paluszny, A., Pentland, C., 2013. Pore-scale imaging and modeling. Adv. Wat. Res. 51, 197–216.
Botan, A., Rotenberg, B., Marry, V., Turq, P., Noetinger, B., 2011. Hydrodynamics in clay nanopores. J. Phys. Chem. C 115, 16109–16115.
Bourg, I.C., Sposito, G., Bourg, A.C.M., 2007. Modeling cation diffusion in compacted water-saturated sodium bentonite at low ionic strength. Environ. Sci. Technol. 41, 8118–8122.
Bourg, I.C., Sposito, G., 2010. Connecting molecular scale to the continuum scale for diffusion processes in smectite-rich porous media. Environ. Sci. Technol. 44, 2085–2091.
Bourg, I.C., Sposito, G., 2011. Molecular dynamics simulations of the electrical double layer on smectite surfaces contacting concentrated mixed electrolyte ($NaCl$-$CaCl_2$) solutions. J. Coll. Interf. Sci. 360, 701–715.
Carminati, A., Schneider, C.L., Moradi, A.B., Zarebanadkouki, M., Vetterlein, D., Vogel, H., Hildebrandt, Weller, U., Schüler, L., Oswald, S.E., 2011. How the rhizosphere may favor water availability to roots. Valdose Zone J. 10, 988–998.
Carminati, A.B., Moradi, D., Vetterlein, P., Vontobel, E., Lehmann, U., Weller, H., Vogel, Oswald, S.E., 2010. Dynamics of soil water content in the rhizosphere. Plant Soil 332, 163–176.
Chávez-Páez, M., Van Workum, K., dePablo, L., dePablo, J.J., 2001. Monte Carlo simulations of wyoming sodium montmorillonite hydrates. J. Chem. Phys. 114, 1405–1413.
Chen, C., Li, W.Z., Song, Y.C., Weng, L.D., Zhang, N., 2012. Formation of water and glucose clusters by hydrogen bonds in glucose aqueous solutions. Comp. Theor. Chem. 15, 85–92.
Chenu, C., 1993. Clay- or sand-polysaccharide associations as models for the interface between micro-organisms and soil: water related properties and microstructure. Geoderma 56, 143–156.
Chu, S.S.C., Jeffrey, G.A., 1968. The refinement of the crystal structures of ß-D-glucose and cellobiose. Acta. Crystallogr. Sect. B 24, 830–838.
Cygan, R.T., Liang, J.-J., Kalinichev, A.G., 2004. Molecular models of hydroxide, oxyhydroxide, and clay phases and the development of a general force field. J. Phys. Chem. B 108, 1255–1266.
Cygan, R.T., Geathouse, J.A., Heinz, H., Kalinichev, A.G., 2009. Molecular models and simulations of layered materials. J. Mater. Chem. 19, 2470–2481.
Ferrage, E., Lanson, B., Sakharov, B.A., Drits, V.A., 2005. Investigation of smectite hydration properties by modeling experimental X-ray diffraction patterns: part I: montmorillonite hydration properties. Amer. Miner. 90, 1358–1374.
Ferrage, E., 2016. Investigation of the interlayer organization of water and ions in smectite from the combined use of diffraction experiments and molecular simulations. A review of methodology, applications, and perspectives. Clays Clay Miner. 64, 346–371.
Fischer, H., Meyer, A., Fischer, K., Kuzyalov, Y., 2007. Carbohydrate and amino acid composition of dissolved organic matter leached from soil. Soil Biol. Biochem. 39, 2926–2935.
Fu, M.H., Zhang, Z.Z., Low, P.F., 1990. Changes in the properties of a montmorillonite-water system during the adsorption and desorption of water: hysteresis. Clays Clay Miner. 486–492.
Grandjean, J., 2001. Interaction of a zwitterionic surfactant with synthetic clays in aqueous suspenions: a multinuclear magnetic resonance study. J. Coll. Interf. Sci. 239, 27–32.
Greenland, D.J., 1965. Interactions between clays and organic compounds in soils. Part II. Adsorption of soil organic compounds and its effect on soil properties. Soils Fert 28, 415–425.
Greenland, DJ., 1956. The adsorption of sugars by montmorillonite I. X-Ray studies. J. Soil Sci. 7, 319–328.
Greenland, D.J., Lindstrom, G.R., Quirk, J.P., 1962. Organic materials which stabilize natural soil aggregates. Proc. Soil Sci. Am. 25, 366–371.
Hallett, P.D., Karim, K.H., Bengough, A.G., Otten, W., 2013. Biophysics of the vadose zone: from reality to model systems and back again. Vadose Zone J. 12. http://dx.doi.org/10.2136/vzj2013.05.0090.
Hellrup, J., Holmboe, M., Nartowski, K.P., Yaroslav, Z., Mahlin, D., 2016. Structure and Mobility of lactose in lactose/sodium montmorillonite nanocomposites. Langmuir 32, 13214–13225.
Hodge, A., 2004. The plastic plant: root responses to heterogeneous supplies of nutrients. New Phytologist. 162, 9–24.
Holmboe, M., Bourg, I.C., 2014. Molecular dynamics simulations of water and sodium diffusion in smectite interlayer nanopores as a function of pore size and temperature. J. Phys. Chem. C 118, 1001–1013.
Holz, M., Heil, S.R., Sacco, A., 2000. Temperature-dependent self-diffusion coefficients of water and six selected molecular liquids for calibration in accurate 1H NMR PFG measurements. Phys. Chem. Chem. Phys. 2, 4740–4742.
Kerisit, S., Liu, C., 2009. Molecular simulations of water and ion diffusion in nano-sized mineral fractures. Environ. Sci. Technol. 43, 777–782.
Laage, D., Hynes, J.T., 2006. A molecular jump mechanism of water orientation. Science 311, 832–835.

Lee, S.G, Choi, J.I.I., Koh, W., Jang, S.S., 2013. Adsorption of β-D-glucose and cellobiose on kaolinite surfaces: density functional theory (DFT) approach. Appl. Clay Sc. 71, 73–81.
Lievens, B., Hallsworth, J.E., Pozo, M.I., Belgacem, Z.B., Stevenson, A., Willems, K.A., et al., 2015. Microbiology of sugar-rich environments: diversity, ecology, and system constrains. Environ. Microbiol. 17, 278–298.
Liu, P., Harder, E., Berne, B.J., 2004. On the calculation of diffusion coefficients in confined fluids and water interfaces with an application to the liquid-vapor interface of water. J. Phys. Chem. B 108, 6595–6602.
Loewenstein, W, 1954. The distribution of aluminum in the tetrahedra of silicates and aluminates. Am. Miner. 39, 92–96.
Marry, V., Rotenburg, B., Turq, P., 2008. Structure and dynamics of water at clay surface from molecular dynamic simulation. Phys. Chem. Chem. Phys. 10, 4802–4813.
Olness, A., Clapp, C.E., 1975. Influence of polysaccharide structure on dextran adsorption by montmorillonite. Soil Biol. Biochem. 7, 113–118.
Paul, E.A., Clark, F.E., 1996. Soil Microbiology and Biochemistry, second ed. Academic Press, New York.
Paynel, F., Pavlov, A., Ancelin, G., Rihouey, C., Picton, L., Lebrun, L., Morvan, C., 2013. Polysaccharide hydrolases are released with mucilages after water hydration of flax seeds. Plant Physiol. Biochem. 62, 54–62.
Pochodylo, A.L., Aoki, T.G., Aristilde, L., 2016. Adsorption mechanisms of microcystin variant conformations at water-mineral interfaces: A molecular modeling investigation. J. Coll. Interf. Sci. 480, 166–174.
Pusino, A., Micera, G., Premoli, A., Gessa, A., 1989. D-glucosamine sorption on Cu(II)-Montmorillonite as the protonated and neutral spcies. Clays Clay Miner. 37, 377–380.
Read, D.B., Gregory, P.J., Bell, A.E., 1999. Physical properties of axenic maize root mucilage. Plant Soil 211, 87–91.
Ryan, P.R., Delhaize, E., Jones, D.L., 2001. Function and mechanism of organic anion exudation from plant roots. Ann. Rev. Plant Physiol. Plant Mole. Biol. 52, 527–560.
Sato, T., Watanabe, T., Otsuka, R., 1992. Effects of layer charge, charge location, and energy change on expansion properties of dioctahedral smectites. Clays Clay Miner. 38, 486–492.
Smaraweera, M., Jolin, W., Vasudevan, D., MacKay, A.A., Gascó, J., 2014. Atomistic prediction of sorption free energies of cationic aromatic amines on montmorillonite: a linear interaction energy method. Environ. Sci. Technol. Lett. 1, 284–289.
Smucker, A.J.M., Park, E.-J., Dorner, J., Horn, R., 2007. Soil micropore development and contributions to soluble carbon transport within microaggregates. Vadose J. 6, 282–290.
Sposito, G., 2013. Green water and global food security. Vadose Zone J. http://dx.doi.org/10.2136/vzj2013.02.0041.
Sposito, G, 1982. Prost R Structure of water adsorbed on smectites. Chem. Rev. 82, 552–573.
Sposito, G., 2008. The Chemistry of Soils, second ed. Oxford University Press, USA.
Sposito, G., 2004. The Surface Chemistry of Natural Particles. Oxford University. Press, Oxford.
Sulman, B.N., Phillips, R.P., Oishi, A.C., Shevliakova, E., Pacala, S.W., 2014. Microbe–driven turnover offsets mineral-mediated storage of soil carbon under elevated CO_2. Nat. Clim. Change 4, 1099–1102 2014.
Sutton, R., Sposito, G., Diallo, M.S., Schulten, H.-R., 2005. Molecular simulation of a model of dissolved organic matter. Environ. Toxicol. Chem. 24, 1902–1911.
Sutton, R., Sposito, G., 2006. Molecular simulation of humic substance-Ca-montmorillonite complexes. Geochim. Cosmochim. Acta 70, 3566–3581.
Sun, H., 1998. COMPASS: an ab initio force-field optimized for condensed phase applications-overview with details on alkane and benzene compounds. J. Phys. Chem. B 102, 7338–7364.
Talekar, S.V., 1977. Temperature dependence of activation energies for self-diffusion of water and of alkali ions in aqueous electrolyte solutions. A model for ion selective behavior of biological. Int. J. Quant. Chem. Quant. Biol. Symp. 4, 459–469.
Tamura, K., Yamada, H., NakawaUnderwood, T., Erastova, V., Cubillas, P., Greenwell, H.C., 2015. Molecular dynamic simulations of montmorillonite-organic interactions under varying salinity: an insight into enhanced oil recovery. J. Phys. Chem. C 119, 7282–7294.
Tertre, E., Delville, A., Prêt, D., Hubert, F., Ferrage, E., 2015. Cation diffusion in the interlayer space of swelling clay minerals—A combined macroscopic and microscopic study. Geochim. Cosmochim. Acta 149, 251–267.
Tinnacher, R., Holmboe, M., Tournassat, C., Bourg, I., Davis, J., 2016. Ion adsorption and diffusion in smectite: molecular, pore, and continuum scale views. Geochim. Cosmochim. Acta 177, 130–149.
Tournassat, C., Chapron, Y., Leroy, P., Bizi, M., Boulahya, F., 2009. Comparison of molecular dynamics simulations with triple layer and modified Gouy-Chapman models in a 0.1 M NaCl-montmorillonite system. J. Coll. Interf. Sci. 339, 533–541.
Tuller, M., Dani, O., Dudley, L.M., 1999. Adsorption and capillary condensation in porous media: liquid retention and interfacial configurations in angular pores. Water Resour. Res. 35, 1949–1964.
Underwood, T., Erastova, V., Cubillas, P., Greenwell, H.C., 2015. Molecular dynamics simulations of montmorillonite-organic interactions under varying salinity: an insight into enhanced oil recovery. J. Phys. Chem. C 119, 7282–7294.
Veneklaas, E.J., Stevens, J., Cawthray, G.R., Turner, S., Grigg, A.M., Lambers, H., 2003. Chickpea and white lupin rhizosphere carboxylates vary with soil properties and enhance phosphorus uptake. Plant Soil 248, 187–197.
van Hees, P.A.W., Jones, D.L., Finlay, R., Godbold, D.L., Lundström, U.S., 2005. The carbon we do not see—the impact of low molecular weight compounds on carbon dynamics and respiration in forest soils: a review. Soil Biol. Biochem. 37, 1–13.
Young, I.M., 1995. Variation in moisture contents between bulk soil and the rhizosheath of wheat (*Triticum aestivum* L. cv. Wembley). New Phytol. 130, 135–139.
Zhang, L., Lu, X., Liu, X., Yang, K., Zhou, J., Zhou, H., 2014. Hydration and mobility of interlayer ions of (Na_xCa_y)-montmorillonite: a molecular dynamics study. J. Phys. Chem. C 118, 29811–29821.
Zhang, L., Lu, X., Liu, X., Yang, K., Zhou, H., 2016. Surface wettability of basal surfaces of clay minerals: insights from molecular dynamics simulation. Energy Fuels 30, 149–160.
Zhao, Q., Burns, S.E., 2013. Modeling sorption and diffusion of organic sorbate in hexadecyltrimethylammonium-modified clay nanopores—A molecular dynamics simulation study. Environ. Sc. Technol. 47, 2769–2776.